Supporting Information

Enhancing the Stability and Emission Efficiency of Circularly Polarized Luminescent Materials for Deep Blue Applications

Si-Fan Lu[a,b], Meng-Na Jing[a], Mian-He Xu[a], Jian Lu[a,c,*], Fa-Kun Zheng[a,b,c], Guo-Cong Guo[a,b,*]

[a] *State Key Laboratory of Structural Chemistry, Fujian Institute of Research on the Structure of Matter, Chinese Academy of Sciences, Fuzhou, Fujian 350002, P. R. China*

[b] *University of Chinese Academy of Science, Beijing, 100049, P. R. China*

[c] *Fujian Science & Technology Innovation Laboratory for Optoelectronic Information of China, Fuzhou, Fujian 350108, P. R. China*

* Corresponding authors' E-mail: *lujian@fjirsm.ac.cn*; *gcguo@fjirsm.ac.cn*

Experimental section

Materials and Chemicals

All the chemicals were purchased from commercial sources and were used without further purification. Ultrapure water was self-prepared and used throughout all experiments. (R)-(+)-2,2'-bis(diphenylphosphino)-1,1'-binaphthalene (*R*-BINAP, 99%), (S)-(-)-2,2'-bis(diphenylphhosphino)-1,1'-binaphthalene (*S*-BINAP, 99%) were purchased from Shanghai Bidepharm Co., Ltd. Methanol (MeOH, 99.9%) were purchased from Shanghai Adamas-beta® Co., Ltd and hydrochloric acid (HCl, 36 wt%) were purchased from Sinopharm Chemical Reagent Co., Ltd.

Synthesis of compounds 1A and 1B

R-CH_3 **1A**:

The organic compounds (R)-(+)-2,2'-bis(diphenylphosphino)-1,1'-binaphthalene (*R*-BINAP, 0.8 mmol, 498.4 mg) was added to a mixed solution of methanol and hydrochloric acid (17 mL, V_{MeOH}: V_{HCl} = 14:3). The solution was then sealed in a 20 mL PTFE-lined stainless steel vessel reactor and then placed into a temperature-controlled oven and heated from room temperature to 120 °C in 60 minutes, maintained at that temperature for 24 hours. After cooling to room temperature and filtering, the filtrate was naturally evaporated in a 100 mL beaker at room temperature for about 10 days to yield colorless rod-like crystals.

The synthetic routines of *S*-CH_3 **1B** is similar to that of **1A**, except that *R*-BINAP is replaced by *S*-BINAP.

X-ray crystallography

Single-crystal X-ray diffractions of compounds **1A** and **1B** were performed by a Rigaku FR-X Microfocus diffractometer equipped with graphite-monochromated Mo-K_α radiation (λ = 0.71073 Å) at 100 K. The intensity data sets were collected using a ω-scan technique and reduced using *CrysAlis*^{Pro} software [1]. The final

structures were refined using a full-matrix least-squares refinement on F^2 with the *Olex*^{2} 1.2 program [2]. The structures were solved by direct methods, and the subsequent successive difference Fourier syntheses yielded other nonhydrogen atoms [3, 4]. All atoms except hydrogen atoms were performed through the anisotropic refinement. The hydrogen atoms were calculated in the idealized positions and refined with riding coordinates on their parent atoms. Pertinent crystal data and structure refinements are summarized in **Table S1**. The hydrogen bond information is shown in **Table S2** and the non-classical hydrogen bond information are shown in **Table S3**. Other non-covalent interactions information is shown in **Tables S4-S5**. And the information of intermolecular interactions is presented in **Table S6**.

Characterization

Powdered X-ray diffraction patterns (PXRD) were recorded with a Rigaku Smartlab X-ray diffractometer equipped with a 1D array detector at 20 kV, 10 mA for Cu-K_α (λ = 1.54178 Å) with a scan speed of 10 deg/min and a step size of 0.02 °, the data were collected within the 2θ range of 5–65°. The *Mercury 2022.3.0* software was utilized to achieve simulated PXRD patterns dependent on the X-ray crystallographic structure (**Fig. S1**). Nuclear magnetic resonance hydrogen (^{1}H NMR) spectra of the samples dissolved in Methanol-D4 were acquired using a Bruker AVANCE III 400 MHz NMR spectrometer (**Fig. S2**). Fourier transform infrared spectra (FT-IR) were measured from 4000 to 400 cm^{-1} using a VERTEX 70 infrared spectrum radiometer (**Fig. S3**). The Raman spectra were measured on a Confocal Raman spectrometer (LabRAM HR) with an excitation wavelength of 633 nm (**Fig. S4**). Thermogravimetric analysis and Differential scanning calorimetry (Tg&DSC) were carried out on a METTLER TOLEDO system at a heating rate of 10 K min^{-1} under nitrogen atmosphere (**Fig. S5**). To investigate the antioxidative properties and durability of chiral materials, the compounds were irradiated with a Xenon lamp for 6 hours. After irradiation, the compounds were characterized using PXRD (**Fig. S7**),

FT-IR (**Fig. S8**), and Raman spectroscopy (**Fig. S9**), and the pre- and post-irradiation changes were compared. Solid-state UV-Vis diffuse reflectance spectroscopy was measured with a Lambda950 (**Fig. S10**). The photoluminescence spectra were recorded on an Edinburgh FLS1000 using a 450 W Xenon lamp as excitation source.

Calculation methods

Geometry optimization was carried out using the B3LYP functional and LANL2DZ [5] basis set in the Gaussian 16 suite of program [6], while DFT calculations were further performed with the CAM-B3LYP hybrid functional [7], and def2-TZVP were chosen as the basis set for C, H, O, P and Cl. The electrostatic potential involved in the analyses was evaluated by Multiwfn and Visual Molecular Dynamics (VMD) based on the highly effective algorithm proposed in Ref [8–10].

The density of states (DOS) and electronic band structures of **1A** and **1B** were calculated using orbital calculations with the DMol3 code in the Materials Studio 2019 software package, employing the Generalized Gradient Approximation of the PW91 functional with the basis set of DNP amending DFT-D of OBS method [11, 12]. The computational model was established based on the original crystal structure file (CIF file), with the removal of crystallization water molecules and the counterion chloride (Cl^-) anions.

Schemes

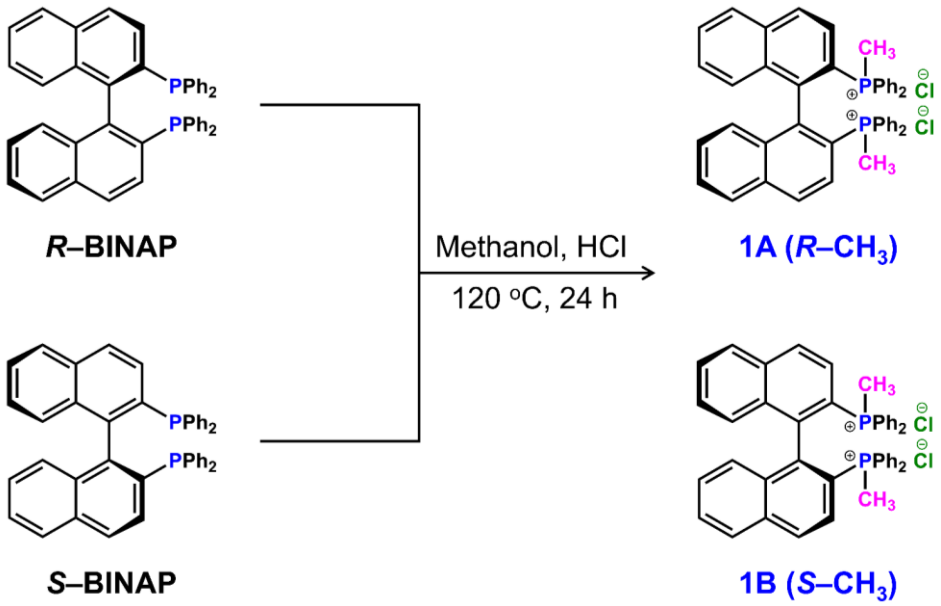

Scheme S1. The synthesis routine of **1A** (*R*-CH_3) and **1B** (*S*-CH_3).

Figures

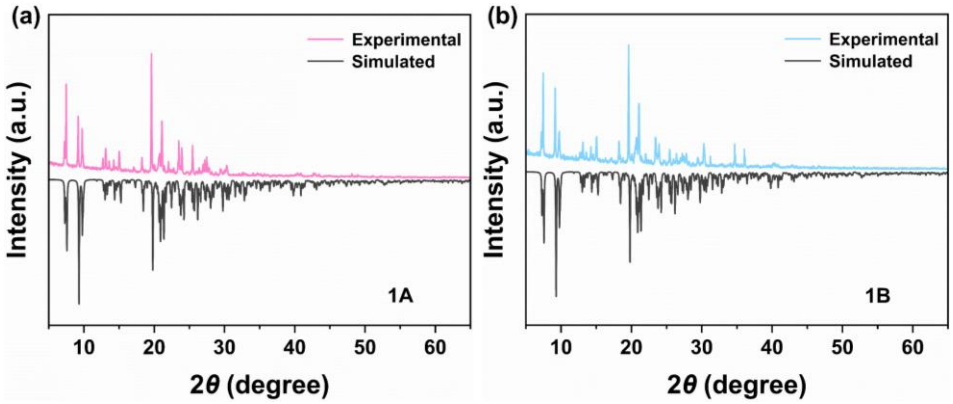

Fig. S1 The PXRD pattern of **1A** (a) and **1B** (b).

Analysis: The PXRD indicate that the diffraction peak positions of compounds **1A** and **1B** within the 5-65° diffraction angle range are in excellent agreement with the theoretical simulation data. This suggests that both substances exhibit high phase purity.

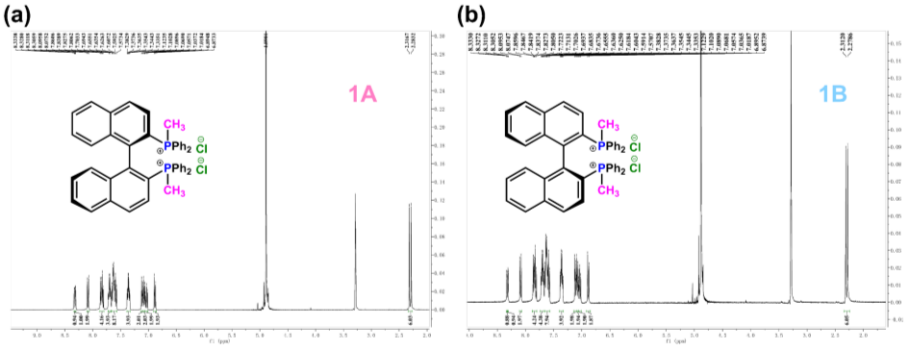

Fig. S2 The ^{1}H NMR spectra of **1A** (a) and **1B** (b) in methanol-d.

Analysis: The chemical shift is related to the residual solvent peak (methanol-d solvent peak position: 7.26 ppm). **1A** ^{1}H NMR (400 MHz, Methanol-d4) δ 8.33 (d, J = 2.3 Hz, 1H), 8.31 (d, J = 2.3 Hz, 1H), 8.09 (d, J = 8.3 Hz, 2H), 7.83 (dd, J = 13.1, 8.6 Hz, 4H), 7.70 (d, J = 3.6 Hz, 4H), 7.66–7.56 (m, 8H), 7.36 (td, J = 7.7, 3.7 Hz, 4H), 7.11 (d, J = 8.3 Hz, 2H), 7.08 (d, J = 8.2 Hz, 2H), 7.06–7.01 (m, 2H), 6.88 (d, J = 8.6 Hz, 2H), 2.30 (d, J = 13.4 Hz, 6H). **1B** ^{1}H NMR (400 MHz, Methanol-d4) δ 8.33 (d, J = 2.3 Hz, 1H), 8.31 (d, J = 2.3 Hz, 1H), 8.09 (d, J = 8.2 Hz, 2H), 7.88–7.80 (m, 4H),

7.70 (td, J = 7.9, 3.8 Hz, 4H), 7.66–7.56 (m, 8H), 7.36 (td, J = 7.7, 3.7 Hz, 4H), 7.11 (d, J = 8.3 Hz, 2H), 7.08 (d, J = 8.4 Hz, 2H), 7.06–7.01 (m, 2H), 6.88 (d, J = 8.5 Hz, 2H), 2.30 (d, J = 13.4 Hz, 6H).

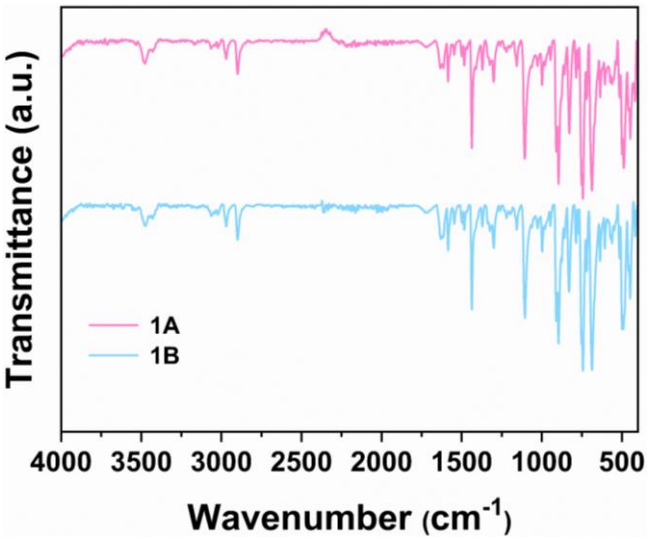

Fig. S3 The FT-IR spectroscopy of **1A** and **1B**.

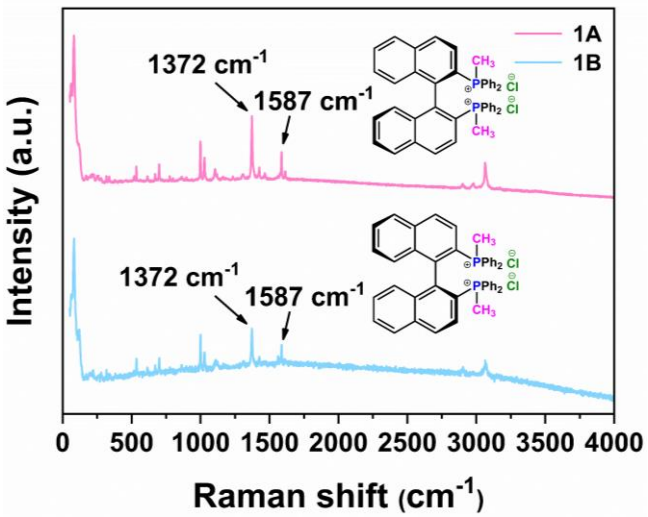

Fig. S4 The Raman spectra of **1A** and **1B**.

Analysis: Raman spectra of **1A** and **1B** were obtained and compared. The Raman peaks of both compounds are in excellent agreement in terms of their positions. Notably, both compounds display a C–H absorption peak at 1372 cm^{-1}, likely corresponding to a methyl group bonded to a phosphorus atom. Furthermore, both compounds exhibit a Raman peak at 1587 cm^{-1}, which is indicative of aromatic

hydrocarbons.

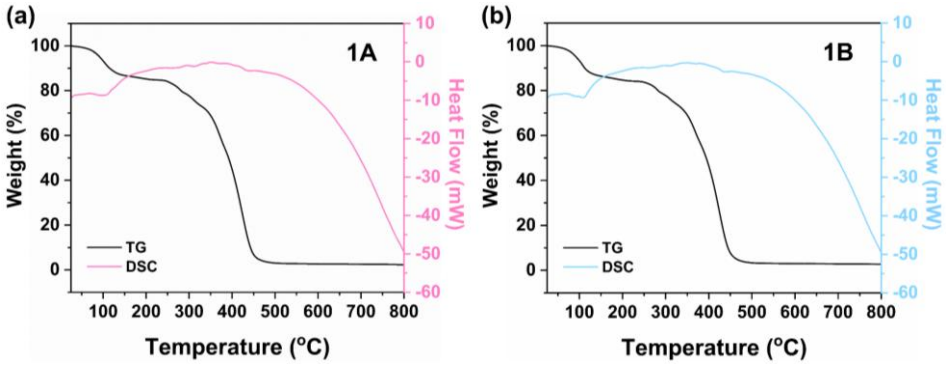

Fig. S5 The Tg&DSC patterns of **1A** (a) and **1B** (b).

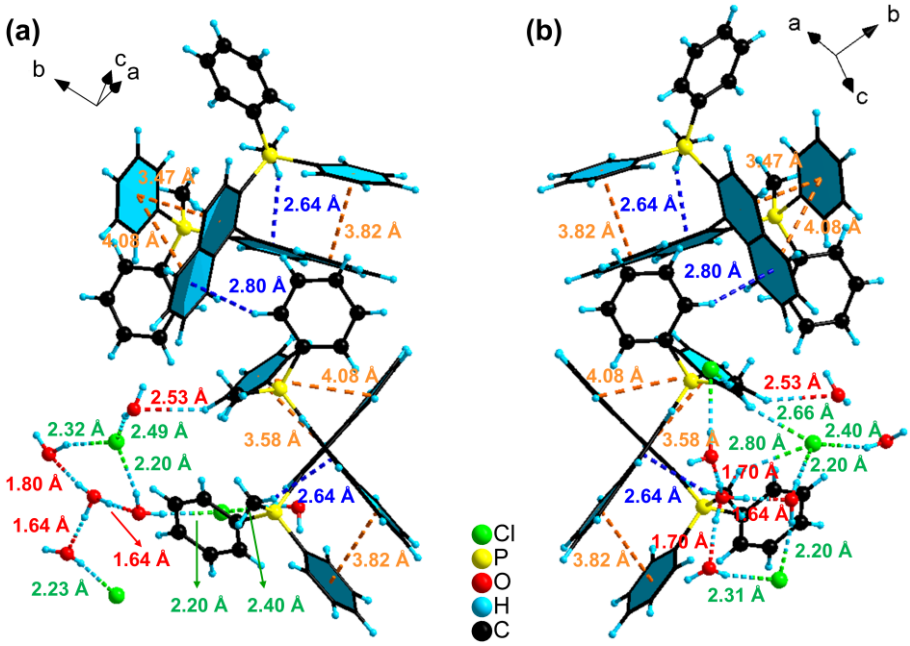

Fig. S6 The partial weak interaction distribution of compounds **1A** (a) and **1B** (b).

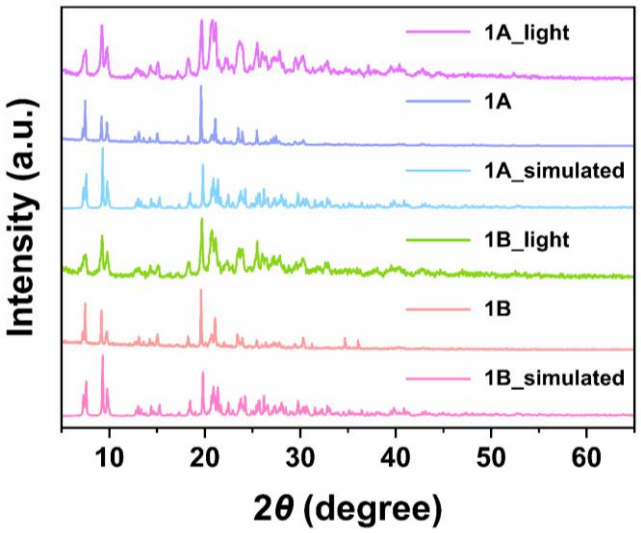

Fig. S7 The PXRD patterns of **1A**, **1B** and **1A**/**1B** after 6 hours of Xenon lamp irradiation, and the corresponding theoretical simulation.

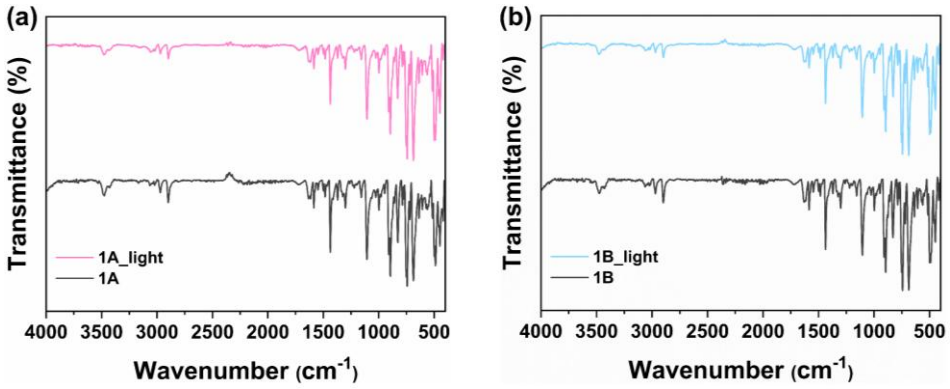

Fig. S8 The FT-IR patterns of **1A** and **1A** after 6 hours of Xenon lamp irradiation (a), and the FT-IR patterns of **1B** and **1B** after 6 hours of Xenon lamp irradiation (b).

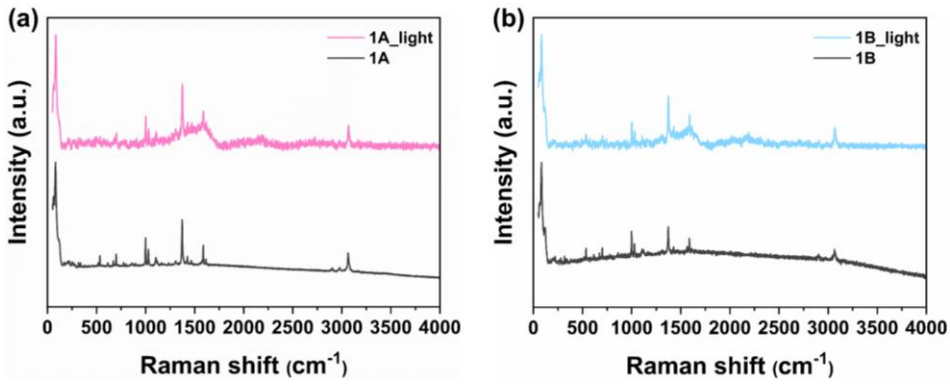

Fig. S9 The Raman patterns of **1A** and **1A** after 6 hours of Xenon lamp irradiation (a), and the Raman patterns of **1B** and **1B** after 6 hours of Xenon lamp irradiation (b).

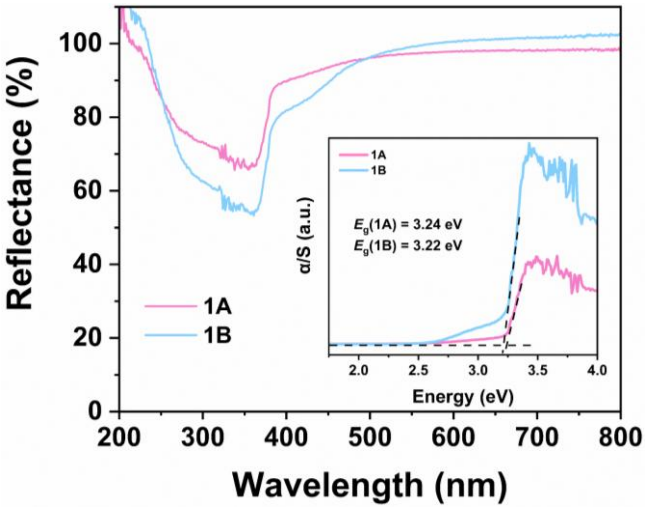

Fig. S10 The solid-state UV-Vis diffuse reflectance spectroscopy of **1A** and **1B**.

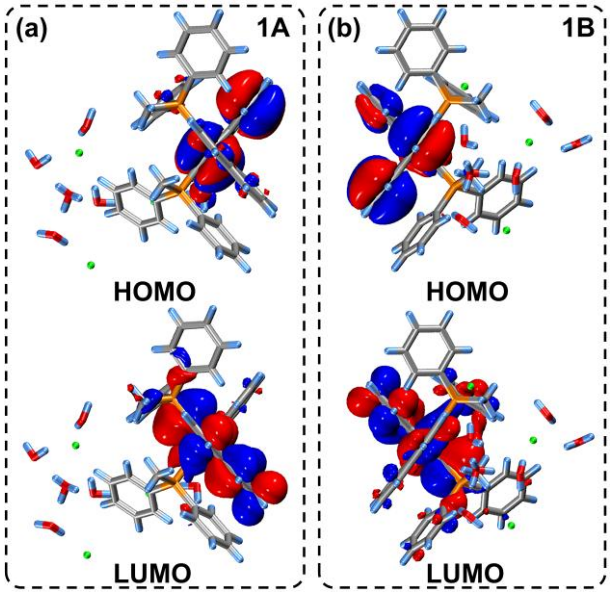

Fig. S11 The molecular orbital distributions of **1A** (a) and **1B** (b) obtained using the Gaussian 16 package [6].

Tables

Table S1. Crystal data and structure refinement of **1A** and **1B**.

	1A	**1B**
CCDC number	2418303	2414162
Empirical formula	$C_{46}H_{51}Cl_3O_6P_2$	$C_{46}H_{51}Cl_3O_6P_2$
Formula weight	868.15	868.15
Temperature/K	100.0	100.0
Wavelength/Å	0.71073	0.71073
Crystal system	orthorhombic	orthorhombic
Space group	$P2_12_12_1$	$P2_12_12_1$
a/Å	13.29590(10)	13.30050(10)
b/Å	13.60120(10)	13.59530(10)
c/Å	24.2603(2)	24.2563(2)
α/°	90	90
β/°	90	90
γ/°	90	90
Volume/Å^3	4387.24(6)	4386.13(6)
Z	4	4
Calcd. density (g cm^{-3})	1.314	1.315
μ/mm^{-1}	0.329	0.329
F(000)	1824	1824
2θ range/°	3.358 to 60.474	3.358 to 60.498
Reflections collected	111394	105977
Data/restraints/parameters	11776/0/538	11739/0/538
Goodness-of-fit on F^2	1.030	1.034
Final R indices [I > 2σ(I)]	R_1 = 0.0313	R_1 = 0.0309
	wR_2 = 0.0875	wR_2 = 0.0836

[a]$R_1 = \sum(F_o - F_c)/\sum F_o$, [b]$wR_2 = [\sum w(F_o^2 - F_c^2)^2/\sum w(F_o^2)^2]^{1/2}$.

Table S2. The classical hydrogen bond information within **1A** and **1B** via *PLATON* software [13].

1A					
D–H	A	d(D–H) (Å)	d(H...A) (Å)	∠DHA	d(D...A) (Å)
O1W–H1WA	O2W	0.85	1.64	176	2.489(3)
O1W–H1WB	O4W	0.85	1.64	171	2.487(2)
O1W–H1WC	O3W	0.75(4)	1.80(4)	171(4)	2.543(3)
C21–H21	O5W	0.95	2.53	138	3.296(3)
C33–H33	O4W	0.95	2.55	139	3.323(3)
1B					
D–H	A	d(D–H) (Å)	d(H...A) (Å)	∠DHA	d(D...A) (Å)
O1W–H1WA	O3W	0.85	1.64	178	2.489(3)
O1W–H1WB	O2W	0.85	1.70	170	2.542(3)
O1W–H1WC	O4W	0.79(5)	1.70(5)	173(5)	2.486(3)
C33–H33	O4W	0.95	2.55	139	3.323(3)
C45–H45	O5W	0.95	2.53	138	3.295(3)

Table S3. The non-classical hydrogen bond information within **1A** and **1B** via *PLATON* software [13].

1A					
D–H	A	d(D–H) (Å)	d(H...A) (Å)	∠DHA	d(D...A) (Å)
O4W–H4WA	Cl2	0.85	2.21	172	3.0501(18)
O4W–H4WB	Cl3	0.85	2.23	172	3.0716(18)
O2W–H2WA	Cl1	0.85	2.20	164	3.0315(18)
O2W–H2WB	Cl2	0.85	2.20	176	3.0428(19)
O008–H00A	Cl2	0.85	2.40	161	3.2195(19)

O008–H00B	Cl3	0.85	2.44	171	3.280(2)
O5W–H5WB	Cl1	0.85	2.49	166	3.319(2)
O3W–H3WA	Cl1	0.85	2.32	160	3.129(2)
O3W–H3WB	Cl3	0.85	2.34	157	3.139(2)
C31–H31A	Cl2	0.98	2.66	152	3.562(2)
C31–H31C	Cl3	0.98	2.68	166	3.635(2)
C44–H44A	Cl2	0.98	2.80	140	3.605(2)
1B					
D–H	A	d(D–H) (Å)	d(H...A) (Å)	∠DHA	d(D...A) (Å)
O4W–H4WA	Cl2	0.85	2.21	171	3.0495(18)
O4W–H4WB	Cl1	0.85	2.23	172	3.0704(18)
O3W–H3WA	Cl3	0.85	2.20	165	3.0298(18)
O3W–H3WB	Cl2	0.85	2.20	175	3.0443(19)
O6W–H6WA	Cl2	0.85	2.40	162	3.2195(19)
O6W–H6WB	Cl1	0.85	2.44	171	3.280(2)
O5W–H5WA	Cl3	0.85	2.49	166	3.317(2)
O2W–H2WA	Cl1	0.85	2.33	159	3.138(2)
O2W–H2WB	Cl3	0.85	2.31	163	3.129(2)
C31–H31C	Cl2	0.98	2.80	140	3.605(2)
C34–H34A	Cl1	0.98	2.68	166	3.635(2)
C34–H34C	Cl2	0.98	2.66	152	3.559(2)

Table S4. The geometrical parameters of C–H…π interaction in **1A** and **1B** via *PLATON* software [13]. (All C–H…π interactions are intramolecular interactions)

X–H(I)…Cg	H…Cg(Å)	H-Perp	Gamma(º)	X–H…Cg(Å)	X…Cg(Å)
1A					
C20–H20…Cg7	2.80	-2.79	1.81	153	3.666(2)
C41–H41…Cg10	2.92	2.82	15.42	125	3.560(2)

C44–H44B…Cg4	2.64	-2.56	14.90	147	3.506(2)
1B					
C13–H13…Cg5	2.80	-2.79	1.79	153	3.666(2)
C31–H31B…Cg3	2.64	2.56	14.86	147	3.505(2)
C41–H41…Cg10	2.93	2.82	15.41	125	3.560(2)

Table S5. The geometrical parameters of π–π interaction in **1A** and **1B** via *PLATON* software [13]. (All π–π interactions are intramolecular interactions.)

Cg(I)-Cg(J)	Cg-Cg(Å)	Alpha(°)	Beta(°)	Gamma(°)	CgI_Perp(Å)	CgJ_Perp(Å)	Slippage(Å)
1A							
Cg1–Cg8	3.4736(13)	15.24(10)	6.6	8.7	-3.4335(8)	3.4506(9)	0.399
Cg3–Cg5	3.8250(13)	13.83(10)	34.9	22.6	3.5317(9)	-3.1360(9)	2.190
Cg5–Cg3	3.8249(13)	13.83(10)	22.6	34.9	-3.1360(9)	3.5317(9)	1.469
Cg7–Cg8	4.0769(13)	16.33(11)	30.6	43.1	-2.9786(9)	3.5100(9)	2.074
Cg8–Cg1	3.4735(13)	15.24(10)	8.7	6.6	3.4506(9)	-3.4334(8)	0.526
Cg8–Cg7	4.0768(13)	16.33(11)	43.1	30.6	3.5100(9)	-2.9786(9)	2.784
Cg8–Cg9	3.5800(12)	15.64(9)	26.6	15.8	3.4447(9)	-3.2013(7)	1.602
Cg9–Cg8	3.5801(12)	15.64(9)	15.8	26.6	-3.2014(7)	3.4447(9)	0.975
1B							

Cg1–Cg7	3.4724(12)	15.24(10)	6.6	8.7	-3.4324(8)	3.4493(9)	0.400
Cg2–Cg6	3.8247(13)	13.83(10)	34.9	22.5	-3.5330(9)	3.1380(9)	2.187
Cg5–Cg7	4.0760(13)	16.32(10)	30.6	43.1	-2.9776(9)	3.5090(9)	2.074
Cg6–Cg2	3.8245(13)	13.83(10)	22.5	34.9	3.1379(9)	-3.5330(9)	1.465
Cg7–Cg1	3.4724(12)	15.24(10)	8.7	6.6	3.4493(9)	-3.4324(8)	0.525
Cg7–Cg5	4.0759(13)	16.32(10)	43.1	30.6	3.5089(9)	-2.9776(9)	2.783
Cg7–Cg9	3.5790(11)	15.63(9)	26.6	15.8	3.4434(9)	-3.2004(7)	1.602
Cg9–Cg7	3.5790(11)	15.63(9)	15.8	26.6	-3.2003(7)	3.4435(9)	0.976

Table S6. The geometrical parameters of intermolecular interaction within **1A** and **1B** via *PLATON* software. [13].

1A					
D–H	A	d(D–H) (Å)	d(H...A) (Å)	∠DHA	d(D...A) (Å)
O1W–H1WA	O2W	0.85	1.64	176	2.489(3)
O1W–H1WB	O4W	0.85	1.64	171	2.487(2)
O1W–H1WC	O3W	0.75(4)	1.80(4)	171(4)	2.543(3)
C21–H21	O5W	0.95	2.53	138	3.296(3)
C33–H33	O4W	0.95	2.55	139	3.323(3)
O4W–H4WA	Cl2	0.85	2.21	172	3.0501(18)
O4W–H4WB	Cl3	0.85	2.23	172	3.0716(18)

O2W–H2WA	Cl1	0.85	2.20	164	3.0315(18)
O2W–H2WB	Cl2	0.85	2.20	176	3.0428(19)
O008–H00A	Cl2	0.85	2.40	161	3.2195(19)
O008–H00B	Cl3	0.85	2.44	171	3.280(2)
O5W–H5WB	Cl1	0.85	2.49	166	3.319(2)
O3W–H3WA	Cl1	0.85	2.32	160	3.129(2)
O3W–H3WB	Cl3	0.85	2.34	157	3.139(2)
C31–H31A	Cl2	0.98	2.66	152	3.562(2)
C31–H31C	Cl3	0.98	2.68	166	3.635(2)
C44–H44A	Cl2	0.98	2.80	140	3.605(2)

1B

D–H	A	d(D–H) (Å)	d(H...A) (Å)	∠DHA	d(D...A) (Å)
O4W–H4WA	Cl2	0.85	2.21	171	3.0495(18)
O4W–H4WB	Cl1	0.85	2.23	172	3.0704(18)
O3W–H3WA	Cl3	0.85	2.20	165	3.0298(18)
O3W–H3WB	Cl2	0.85	2.20	175	3.0443(19)
O6W–H6WA	Cl2	0.85	2.40	162	3.2195(19)
O6W–H6WB	Cl1	0.85	2.44	171	3.280(2)
O1W–H1WA	O3W	0.85	1.64	178	2.489(3)
O1W–H1WB	O2W	0.85	1.70	170	2.542(3)
O5W–H5WA	Cl3	0.85	2.49	166	3.317(2)
O2W–H2WA	Cl1	0.85	2.33	159	3.138(2)
O2W–H2WB	Cl3	0.85	2.31	163	3.129(2)
O1W–H1WC	O4W	0.79(5)	1.70(5)	173(5)	2.486(3)
C31–H31C	Cl2	0.98	2.80	140	3.605(2)
C33–H33	O4W	0.95	2.55	139	3.323(3)
C34–H34A	Cl1	0.98	2.68	166	3.635(2)
C34–H34C	Cl2	0.98	2.66	152	3.559(2)
C45–H45	O5W	0.95	2.53	138	3.295(3)

References

[1] *Rigaku Oxford Diffraction, CrysAlisPro software system, version v40.67a*, Rigaku Corporation, Oxford, UK, 2019.

[2] O. V. Dolomanov, L. J. Bourhis, R. J. Gildea, J. A. Howard and H. Puschmann, OLEX2: a complete structure solution, refinement and analysis program, *J. Appl. Cryst.*, 2009, **42**, 339-341.

[3] G. M. Sheldrick, SHELXT–Integrated space-group and crystal-structure determination, *Acta Crystallogr. A.*, 2015, **71**, 3-8.

[4] G. M. Sheldrick, A short history of SHELX, *Acta Crystallogr. A.*, 2008, **64**, 112-122.

[5] S. Asghari, I. Mohammadpoor-Baltork, H. Sabzyan, S. Tangestaninejad, M. Moghadam and V. Mirkhani, Experimental and computational insights into the iodine vapor capture by imine-and amine-linked covalent organic frameworks, *J. Environ. Chem. Eng.*, 2024, **12**, 114763.

[6] Gaussian 16, Revision C.01, M. J. Frisch, G. W. Trucks, H. B. Schlegel, G. E. Scuseria, M. A. Robb, J. R. Cheeseman, G. Scalmani, V. Barone, G. A. Petersson, H. Nakatsuji, X. Li, M. Caricato, A. V. Marenich, J. Bloino, B. G. Janesko, R. Gomperts, B. Mennucci, H. P. Hratchian, J. V. Ortiz, A. F. Izmaylov, J. L. Sonnenberg, D. Williams-Young, F. Ding, F. Lipparini, F. Egidi, J. Goings, B. Peng, A. Petrone, T. Henderson, D. Ranasinghe, V. G. Zakrzewski, J. Gao, N. Rega, G. Zheng, W. Liang, M. Hada, M. Ehara, K. Toyota, R. Fukuda, J. Hasegawa, M. Ishida, T. Nakajima, Y. Honda, O. Kitao, H. Nakai, T. Vreven, K. Throssell, J. A. Montgomery, Jr., J. E. Peralta, F. Ogliaro, M. J. Bearpark, J. J. Heyd, E. N. Brothers, K. N. Kudin, V. N. Staroverov, T. A. Keith, R. Kobayashi, J. Normand, K. Raghavachari, A. P. Rendell, J. C. Burant, S. S. Iyengar, J. Tomasi, M. Cossi, J. M. Millam, M. Klene, C. Adamo, R. Cammi, J. W. Ochterski, R. L. Martin, K. Morokuma, O. Farkas, J. B. Foresman, and D. J. Fox, Gaussian, Inc., Wallingford CT, 2016.

[7] T. Yanai, D. P. Tew and N. C. Handy, A new hybrid exchange–correlation functional using the Coulomb-attenuating method (CAM-B3LYP), *Chem. Phys. Lett.*, 2004, **393**, 51-57.

[8] T. Lu and F. Chen, Multiwfn: A multifunctional wavefunction analyzer, *J. Comput. Chem.*, 2012, **33**, 580-592.

[9] J. Zhang and T. Lu, Efficient evaluation of electrostatic potential with computerized optimized code, *Phys. Chem. Chem. Phys.*, 2021, **23**, 20323-20328.

[10] T. Lu and F. Chen, Quantitative analysis of molecular surface based on improved Marching Tetrahedra algorithm, *J. Mol. Graph. Model.*, 2012, **38**, 314-323.

[11] B. Delley, An all-electron numerical method for solving the local density functional for polyatomic molecules, *J. Chem. Phys.*, 1990, **92**, 508-517.

[12] B. Delley, From molecules to solids with the DMol3 approach, *J. Chem. Phys.*, 2000, **113**, 7756-7764.

[13] A. Spek, Single-crystal structure validation with the program PLATON, *J. Appl. Crystallogr.*, 2003, **36**, 7-13.